INTERNATIONAL JOURNAL OF
COASTAL & OFFSHORE ENGINEERING IJCOE Vol.3 /No. 4/Winter 2018 (1-11)

Available online at: http://ijcoe.org/browse.php?a_code=A-10-89-1&sid=1&slc_lang=en

Numerical Study on Hydrodynamic Force and Wave Induced Vortex Dynamics around Cylindrical Pile

Mohammad Mohammad Beigi kasvaei[1], Mohammad Hossein Kazeminezhad[2*], Abbas Yeganeh-Bakhtiary[3]

[1] *PhD Candidate, Iranian National Institute for Oceanography & Atmospheric Science, Tehran, Iran; mmbeigi@inio.ac.ir*
[2*] *Corresponding Author: Assistant Professor, Iranian National Institute for Oceanography & Atmospheric Science, Tehran, Iran; mkazeminezhad@inio.ac.ir*
[3] *Associate Professor, School of Civil Engineering, IUST, Tehran, Iran; yeganeh@iust.ac.ir*

ARTICLE INFO

Article History:
Received: 30 Aug. 2017
Accepted: 5 Mar. 2018

Keywords:
Keulegan-Carpenter (KC) number
OpenFOAM
RANS Equations
Vortex Shedding
Wave-Pile Interaction

ABSTRACT

Three-dimensional numerical simulation of regular waves passing over cylindrical monopile was conducted to investigate the hydrodynamic forces and vortex dynamics. The rectangular wave flume and monopile were modeled with a solver; available in the open-source CFD toolkit OpenFOAM®. This solver applies the Reynolds-Averaged Navier-Stokes (RANS) equations with the volume of fluid technic (VOF) for tracking free surface. To validate numerical model, results were compared to experimental data, and admissible agreement was seen. Computations were done for four cases with different wave characteristics consequently for different Keulegan-Carpenter (KC) numbers. In-line force acting on pile was studied and the results indicated that the total in-line force was influenced as the KC number varied. The vortex dynamics around the pile was also investigated by means of the Q criterion and vorticity field. Furthermore, variation of bed shear stress around the pile was investigated; it was concluded that the bed shear stress was influenced by KC number which is the result of existence of horseshoe vortices. The bed shear stress near the pile was negative due to existing of the horseshoe vortex. It began when KC exceeds 6; while by increasing KC up to 20, the magnitude of negative values of bed shear stress near the pile increase which implied the horseshoe vortices were completely formed.

1. Introduction

Cylindrical piles are widely used in marine structures such as offshore wind turbine monopiles, offshore platform legs and jetty piers. These structures are subjected to waves with different conditions. Cylindrical piles regarding their dimensions and wave characteristics are categorized in slender, intermediate and large piles. This can be demonstrated by means of Keulegan-Carpenter (KC) number as:

$$\mathrm{KC} = \frac{U_m T}{D} \tag{1}$$

where U_m is the maximum of wave orbital velocity, T is wave period and D is the pile diameter. For the slender piles the flow field changes significantly with the increase of disturbance around the pile. At upstream of the pile, the horseshoe vortex is formed due to rotation in the incoming flow; the lee side vortices are caused by the rotation in the boundary layer over the surface of the pile [1]. For the intermediate piles, the turbulence around them is more complex. Existence of vortices around the pile affects the wave force acting on the pile which is one of the most criteria in pile design [2]. Consequently, a great deal of effort is required to investigate the vortex dynamics around the pile. For the large piles, flow does not separate, hence no vortices occur; while, reflection and diffraction occur [1]. It is beyond the scope of this paper to investigate on the large piles.

Due to the importance of wave-pile interaction, both physical and numerical modeling of the wave-pile interaction has been of great interest in the last decades. Sumer et al. [1] carried out vast experiments on flow passing over vertical cylinders as well as the wave induced vortex shedding around vertical cylinders. A range of different KC numbers is used to investigate its influence on different parameters around the pile e.g. vortices and bed shear stress.

Iwagaki and Ishida [2] conducted an experimental study on wake vortices and pressure distribution around a circular cylinder under oscillatory motion. It is concluded that the wave pressures around a cylinder are affected by both wake vortices and the dynamic pressure.

As mentioned before, numerical modelling of wave induced flow and hydrodynamic forces over pile also carried out in the literature [3-11]. Wave forcing from steep and fully nonlinear regular stream function waves on slender piles is computed by Paulsen et al. [12]. Jiang et al. [13] numerically studied the solitary waves propagating over a cylindrical pile to investigate wave loads and vortices. Haddorp [14] carried out literature review and analytical study on flow regime and scour around cylindrical pile. In order to categorize the flow regime around a vertical pile, a graph was presented based on Sumer and Fredsoe's [15] investigations. The graph shows three flow regimes or three pile categories as illustrated in Figure 1. As seen, KC= 1 and KC= 6 are the borders for categorizing between large, intermediate and slender pile, respectively. Moreover, it indicates that from KC= ∞ (current flow) to KC= 6, horseshoe vortices exist and KC= 1 is the limit state of existing lee-wake vortices. Based on Hoffmans and Verheij [16] and Coastal Engineering Manual [17], diffraction and reflection are significant when D/L > 0.1; however, Sumer and Fredsoe [15] and Isaacson [18] maintained D/L > 0.2 as the limit state for the diffraction limit.

Short literature review revealed that, some studies have been carried out on waves and pile interaction. However, few studies have been conducted on the wave force acting on the pile and vortex dynamics considering the slender and intermediate piles categories objectively. The main aim of the study presented in this paper is to investigate on the wave force acting on the pile and vortex dynamics around that and the effect of KC number on them, especially for slender pile, intermediate pile and when it is located in the borderline between slender and intermediate. The open source CFD code of OpenFOAM® is implemented to simulate non-breaking regular waves passing over the pile. The multiphase, Eulerian solver (interFoam) is applied to solve the governing equations. First, numerical results were compared to the experimental ones to validate the model. Then, four cases with different KC numbers were simulated to investigate hydrodynamic wave force, vortex dynamics and bed shear stress.

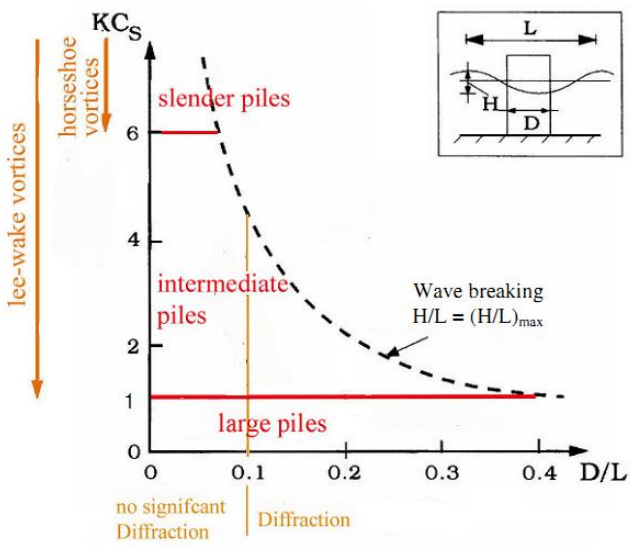

Figure 1. Demonstration of the flow regimes according to KC and *D/L*, adopted from [14]

2. Numerical Method

2.1. Governing Equations

Reynolds averaged Navier–Stokes equations (RANS) coupled with the continuity equation for incompressible flows in Cartesian coordinates are considered as the governing equations for the flow as follows:

$$\frac{\partial U_i}{\partial t}+\frac{\partial\left(U_iU_j\right)}{\partial x_i} = -\frac{1}{\rho}\frac{\partial P}{\partial x_i}+\frac{\partial}{\partial x_i}\left[\frac{\mu_{eff}}{\rho}\left(\frac{\partial U_i}{\partial x_j}+\frac{\partial U_j}{\partial x_i}\right)\right]+g_i-\frac{\partial\left(\overline{u_i'u_j'}\right)}{\partial x_j} \quad (2)$$

$$\frac{\partial U_i}{\partial x_i}=0 \quad (3)$$

where U_i denotes the mean fluid velocity component in the i-th direction, P is the pressure, ρ is the fluid density, g_i denotes the acceleration of gravity, u' denotes the fluctuating velocity component, $\mu_{eff}=\mu+\mu_t$, μ is the molecular viscosity, and μ_t is the turbulent eddy viscosity.

The Shear Stress Transport (SST) k-ω turbulence model is employed as the turbulence closure [19]. The turbulent kinetic energy k and the specific dissipation rate ω are expressed as

$$\frac{\partial(\rho k)}{\partial t}+\frac{\partial\left(\rho U_j k\right)}{\partial x_j}=P_k-\beta^*\rho\omega k+\frac{\partial}{\partial x_j}\left[\left(\mu+\sigma_k\mu_t\right)\frac{\partial k}{\partial x_j}\right] \quad (4)$$

$$\frac{\partial(\rho\omega)}{\partial t}+\frac{\partial\left(\rho U_j\omega\right)}{\partial x_j}=\frac{\gamma}{\upsilon_t}P_k-\beta\rho\omega^2+\frac{\partial}{\partial x_j}\left[\left(\mu+\sigma_k\mu_t\right)\frac{\partial\omega}{\partial x_j}\right]+2\left(1-F_1\right)\frac{\rho\sigma_{\omega2}}{\omega}\frac{\partial k}{\partial x_j}\frac{\partial\omega}{\partial x_j} \quad (5)$$

here F_1 is a harmonic function expressed as

$$F_1=\tanh\left\{\min\left[\max\left(\frac{\sqrt{k}}{\beta^*\omega d},\frac{500\nu}{d^2\omega}\right),\frac{4\rho\sigma_{\omega2}k}{CD_{k\omega}d^2}\right]\right\}^4 \quad (6)$$

$$CD_{k\omega}=\max\left(2\rho\sigma_{\omega2}\frac{1}{\omega}\frac{\partial k}{\partial x_j}\frac{\partial\omega}{\partial\omega j},10^{-10}\right) \quad (7)$$

and $\nu_t=\mu_t/\rho$ is the turbulent kinematic viscosity, μ_t is computed as:

$$\mu_t=\frac{\rho a_1 k}{\max\left(a_{1\omega},\Omega F_2\right)} \quad (8)$$

$$F_2=\tanh\left[\max\left(2\frac{\sqrt{k}}{\beta^*\omega d},\frac{500\nu}{d^2\omega}\right)\right]^2 \quad (9)$$

where d is the distance between the field point and the nearest wall, and Ω is the vorticity magnitude.

Turbulence model constants are $\sigma_{k1}=0.85034$, $\sigma_{k2}=1.0$, $\sigma_{\omega1}=0.5$, $\sigma_{\omega2}=0.85616$, $\beta_1=0.075$, $\beta_2=0.0828$, $\beta^*=0.09$, $a_1=0.31$, $\gamma_1=5/9$ and $\gamma_2=0.4403$ [19, 20].

The free surface is traced by the VOF technique [21]. The governing equations of the flow and transport equation for the volume fraction of water were solved by a Finite Volume Method, in which the equations were integrated over the control volume and time.

2.2. Computational Domain and Boundary Conditions

A numerical rectangular shape wave tank was modelled, as shown in Figure 2. Dimensions were l_x, l_z and h in X, Z and Y directions, respectively. Pile diameter is demonstrated as D and water depth equals to d. As illustrated in Figure 2, no-slip wall boundary condition was considered for bottom of the wave tank, since flow velocity is zero in all directions. Slip wall boundary condition also was implemented for the side walls (front and back in OpenFOAM modelling) and ceiling of the tank [7]. Pile was located at specific distance away from left boundary of tank and no-slip wall boundary condition was considered for the hydraulically smooth pile face. Wave inlet was located at the left-hand side of the wave tank. At the inlet, regular waves using Airy theory as surface elevation were generated. As the wave tank was long enough for all the cases, waves can develop along that and can reach the real shape. At the outlet, a wave damping (relaxation zone) technique was performed which adequately stamps out reflections in the wave tank [4]. A toolbox of waves2Foam [7, 22] was adopted to generate and absorb free surface water waves. Waves2Foam applies the VOF and the relaxation zone technique (active sponge layers) to the 'InterFoam' multiple phase solver.

The "blockMesh" utility was used for mesh generation. Computational domain was divided to eight blocks. Total number of cells was O (10^5) in the modelling. Non-uniform mesh was used with relatively fine mesh close to the pile and bed to fully consider the wall boundary impact on numerical modelling. The finest grid next to the pile was about 0.01 of the pile diameter. Meshes were totally hexahedral and parallel to the stream lines. The numerical model was run with several forms of meshing to obtain the optimum one. The model results are not significantly sensitive to the selected mesh form and cells sizes. Figure 3 shows the general view of the applied mesh.

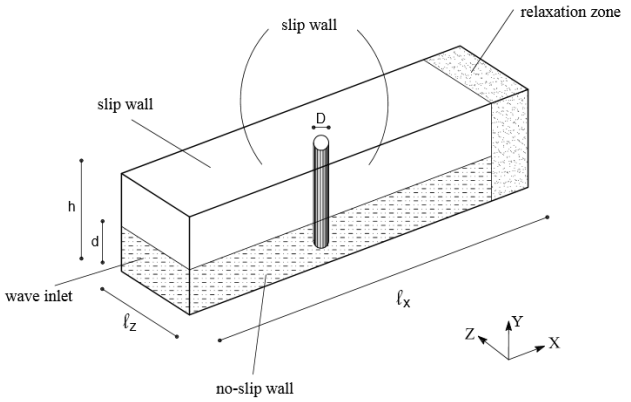

Figure 2. Computational domain and boundary conditions (not scale)

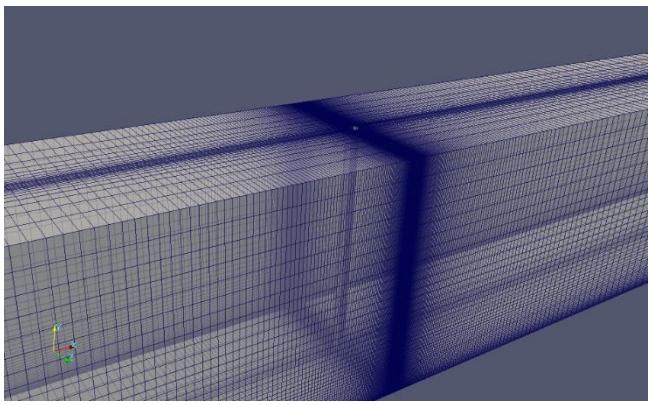

Figure 3. A view of applied mesh around the pile

3. Model Validation

Prior to investigate the effects of KC number on hydrodynamic force acting upon and vortex dynamics around the vertical pile, model validation was carried out using experimental data of Mo et al. [6]. The experiments conducted in the Large Wave Flume (GKW) of Coastal Research Centre (FZK) in Hannover, Germany. This wave flume has an effective length of 309 m, a width of 5 m and a depth

of 7 m. A steel circular cylinder with a diameter of 0.7 m was instrumented and installed in the flume. In order to simulate above mentioned experimental condition, total length of numerical flume in the direction of wave propagation was considered l_x= 77 m to reduce the computational costs, while other dimensions were as experimental conditions. Pile diameter (D) was 0.7 m and located at 40 m away from the wave inlet (left boundary). Wave height and wave period were 1.2 m and 4 s, respectively and KC number was 6.13. For mesh generation, blockMesh utility of OpenFOAM was used and all meshes were hexahedral with total number of about 433,000. Boundary conditions were the same as the other cases as described in section 3. Simulation was conducted for 40 s which means 10 waves were generated and passed over the pile.

For model validation, some numerical results were compared to experimental ones. Comparison of simulated and measured nondimensional in-line force acting on the pile is presented in Figure 4. The wave forces on the pile was predicted by integrating the pressure and viscous stresses along the pile in a discretized manner. The pressure and viscous forces from each cell face on the surface of the pile were summed to find the total pressure and viscous forces, respectively. As seen from the figure, there is a good agreement between the numerical results and the experimental ones. Thus, the numerical model can predict the hydrodynamic force acting on the pile well. Figure 5 illustrates water particle velocity for both numerical simulation and experimental results at wave gauge located at x=40 m near the side wall in two different levels (y/d= -0.32 and y/d= -0.57, y is distance from still water level and d is water depth). The particle velocity was nondimensionalized by dividing it to the phase velocity of the wave. In both levels, acceptable agreement was seen between the numerical results and the experimental ones. In addition, time histories of dynamic pressure along the half perimeter of the pile in six angular points at y/d= -0.11 are depicted in Figure 6. As seen, the numerical results conform closely with experimental results. Since generated vortices around the pile affect the pressure field, by obtaining acceptable results in modeling of pressure field, it is expected that the numerical model performs well in simulation of vortex dynamics as well.

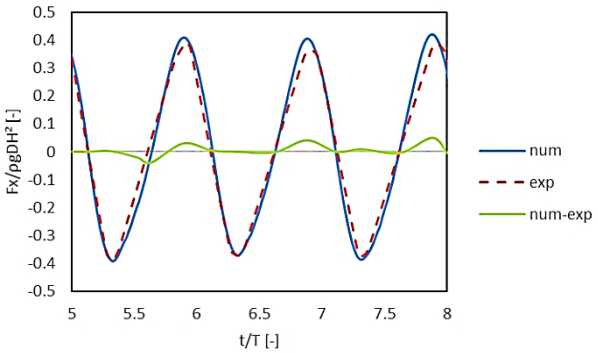

Figure 4. Total in-line force acting upon pile in numerical model and experimental results

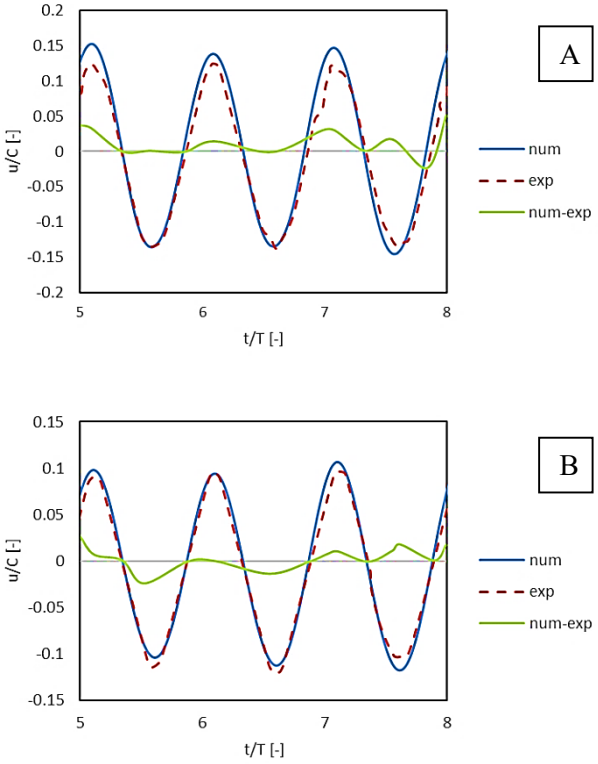

Figure 5. Water particle velocity at wave gauge location with coordinate $x = 40\text{m}$ near the side wall in two different levels (A) $y/d = -0.32$ (B) $y/d = -0.57$

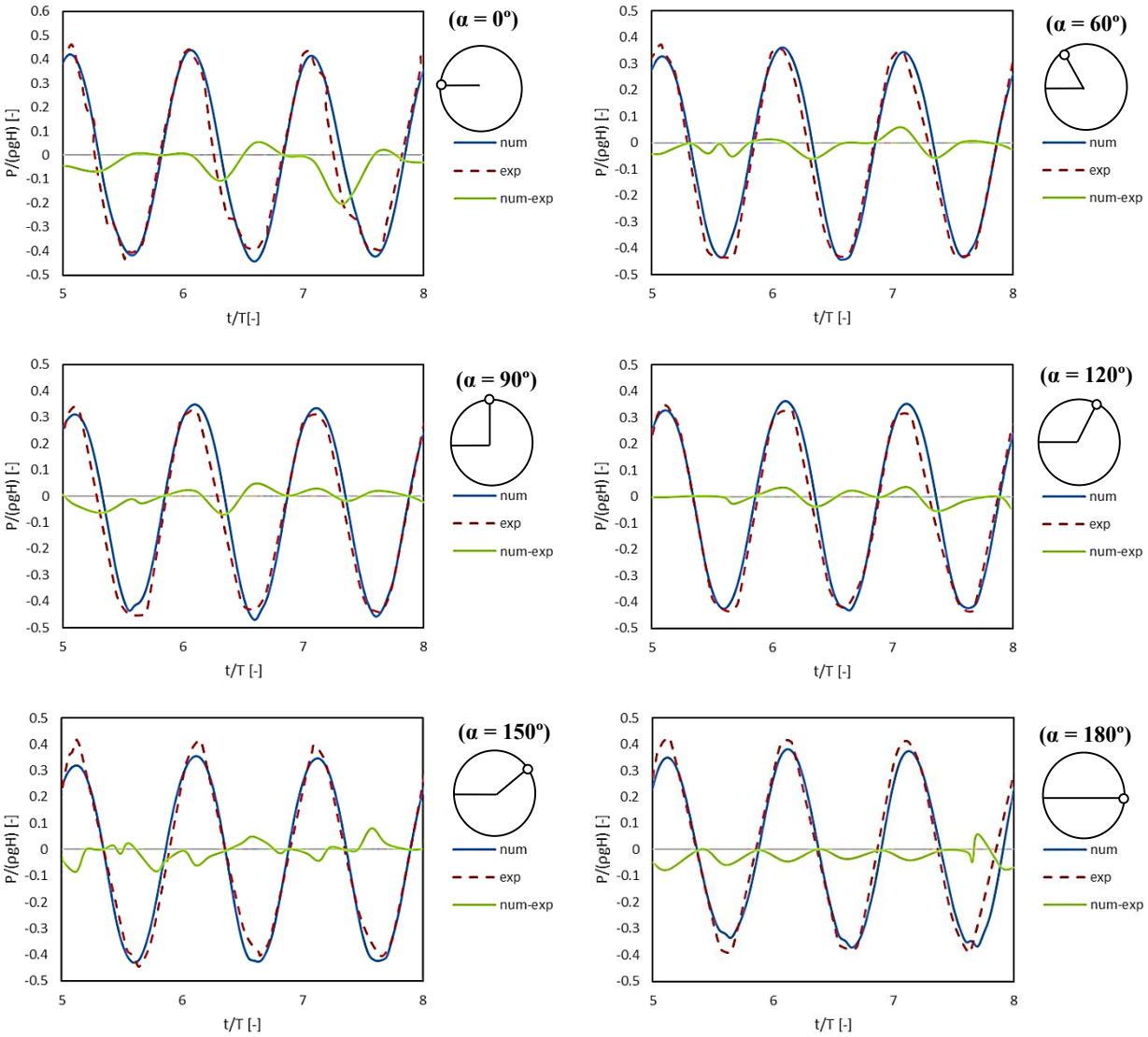

Figure 6. Time histories of dynamic pressure along the perimeter of the pile at in six angular points at y/d= -0.11

Although, the free surface study is not the main goal of this paper, due to the presence of the wave and the wave-pile interaction, accuracy in free surface modelling is also required. Therefore, the numerical results and experimental data for the surface elevation at four wave gauges are presented and compared in Figure 7. The reference wave amplitude in Figure 7 is the maximum elevation of WG 11, which is located near the side wall at x = 40 m. The other three wave gauges are located close to the pile face which locations are shown for every single graph on its top. As it is shown good agreement were seen among numerical results and those of the experiments. This approved that the use of Airy wave theory in wave inlet does not affect the results, which is due to the fact that the wave develops along the flume. For WG_{cyl} 1 which is located in frontline of the pile, it is seen that the numerical model tends to overestimate the wave trough passed the pile, which can be attributed to disturbance in front of the pile.

4. Result and Discussion

Four cases of experimental studies of Sumer et al. [1] with different wave characteristics are numerically modelled to investigate the influence of KC number on the hydrodynamic forces acting on pile and vortex dynamics around the pile. In all four cases wave tank dimensions were equal to l_x= 26.5 m, l_z= 0.6 m and h= 0.8 m. Table 1 presents the wave and the pile characteristics. Pile diameter and water depth were respectively 0.04 and 0.4 m. A multi block hexahedral mesh with 560,000 total number of cells was generated by blockMesh utility. The simulations were carried out for 10 waves period. All aspects of numerical method including consistency, stability, convergence, accuracy and mesh dependency on the results were considered during the simulations.

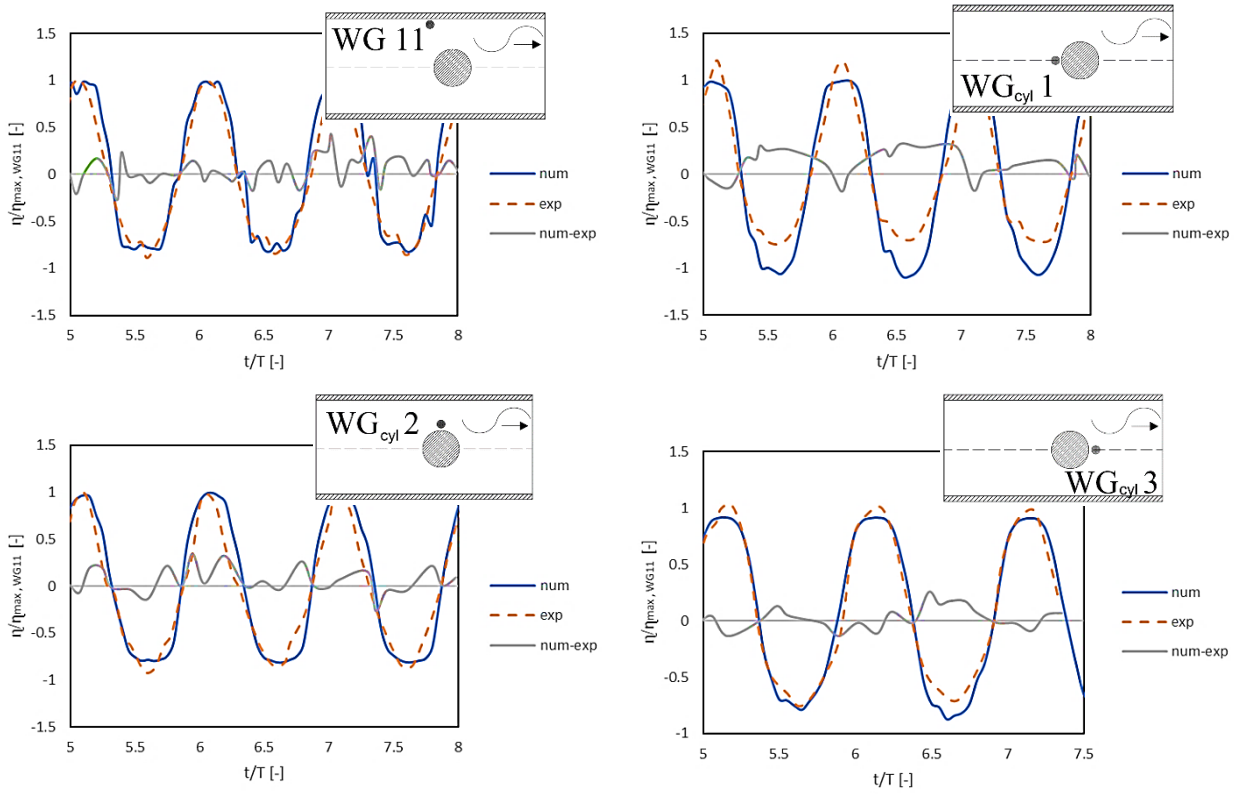

Figure 7. Time histories of surface elevation at 4 different wave gauges

Table 1. Wave and pile characteristics in simulations

Case No.	Water depth (*d*) [m]	Wave height (*H*) [m]	Wave period (*T*) [sec]	Pile diameter (*D*) [m]	*KC* number [-]
1	0.4	0.024	2.2	0.04	2.8
2	0.4	0.023	4.4	0.04	6.1
3	0.4	0.039	4.4	0.04	10.3
4	0.4	0.08	4.4	0.04	20.1

4.1. Hydrodynamic Force

When a pile is exposed to incident waves, depend on the size of circular pile and wave characteristics, the flow field disturbance is different. Hydrodynamic forces acting on pile can be estimated by Morison's equation. It can be said Morison's equation is valid when $D/L<0.2$ (L is the wave length and D is the pile diameter) [23]. In addition to D/L, KC number is significant in the calculation of hydrodynamic forces acting on pile. In the above-mentioned cases $D/L<0.2$, while the related KC numbers are in three ranges: KC<6.0 (Case 1), KC≈ 6 (Case 2) and KC>6 (Cases 3-4). It is expected that the flow pattern and the hydrodynamic force affected by the KC variations.

The time series of total hydrodynamic in-line force acting on the pile for all cases with different KC numbers are depicted in Figure 8. As seen, variation of KC number influences on the hydrodynamic in-line force. According to Eq. (1), KC may change by variation in U_m, T or D. As seen in Table (1), in all four cases D and T are not changed, except for case 1. Therefore, for case 1, KC change due to change in T and for case 2, 3 and 4, KC change due to change in U_m, which is result of change in H. Comparing results for case 1 and 2 showed that change in KC due to change in T is not significantly influence on the in-line force on pile. While, for case 2, 3 and 4, in which change in KC is due to change in H, the in-line force increased remarkably by increasing KC. In Case 4 (KC= 20.1) which is in vortex shedding regime [9] (will be explained extensively in the next section), three pick points in negative values of force can be seen. These are due to vortex shedding behind the pile and consequently increasing of turbulence intensity around the pile.

As seen from Figure 8, in case 4 (cnoidal wave theory characteristics), the absolute value of the wave forces in the crest half period are larger than the absolute value of the wave forces in the trough half period. This is due to the fact that cnoidal waves have a sharp crests and very flat troughs [17].

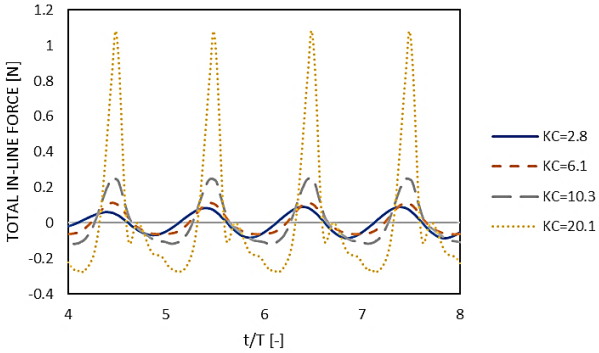

Figure 8. Time series of total hydrodynamic in-line force acting upon pile for all cases with different KC number

Figure 9 illustrates relation between the drag force to the inertia force components [23]. In the graph,

positions of the studied cases are specified by different symbols. It is obvious that for Case 1 (KC= 2.8) the inertia force component is dominant, and is 2 times larger than the drag force component. For Case 2 (KC= 6.1) red rectangle is located on border line and for Cases 3 and 4 that KC exceeds than 6, symbols are located in region, in which the inertia force component is equal to drag force component. As expected for small KC number condition inertia force is dominant, on the other hand for large KC number drag force is dominant. Recalling the Figure 1 ([14]'s graph), it is seen that case 1 belongs to intermediate pile region, while cases 3 and 4 belong to slender pile. Case 2 is near border line of intermediate and slender pile. It can be concluded that, for intermediate piles drag force component is half of inertia force component and for slender piles those components are equal. Fully developed vortices affected velocity field and then resulted in pressure field which might cause to increase the drag force. These were along with experimental data stated that wave pressures around a cylinder are affected by wake vortices [2]. Also, these vortices induce local pressure depressions in the wave field.

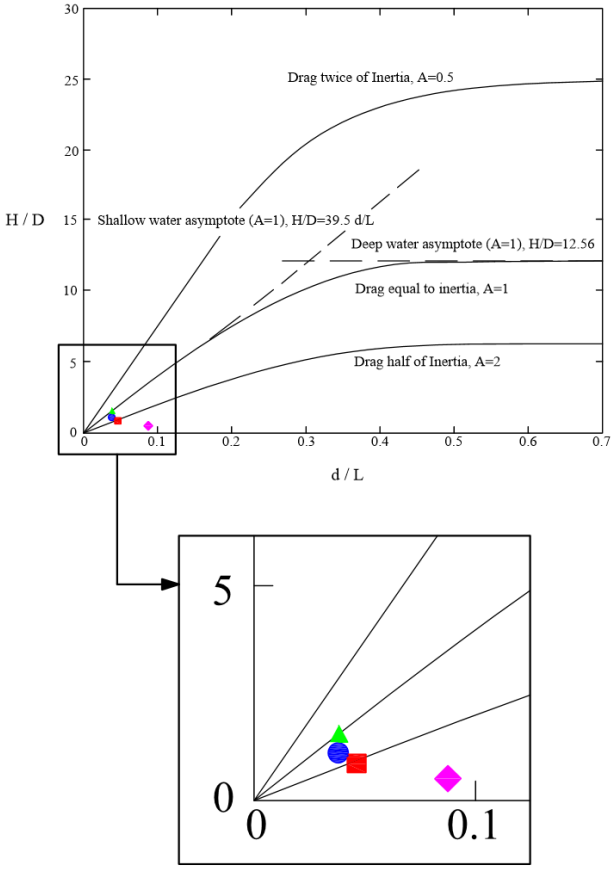

Figure 9. Relative magnitude of inertia and drag forces for cylinders with *D/L* < 0.2 [23]
Case 1 ◆, case 2 ■, case 3 ●, case 4 ▲

4.2. Vortex Dynamics

The vortex dynamics, related to horseshoe vortices, lee-wake vortices and vortex shedding are evaluated by means of Q criterion, vorticity and amplification factor of bed shear stress (α). The vorticity has been using in numerous studies to show vortex shedding around a structure. However, due to its weakness to distinguish between vortex cores and shear motions, the vorticity method can be replaced by other criteria, e.g. the Q criterion, the Δ criterion, the λ_{ci} criterion, and the λ_2 criterion [24]. These methods are formulated based on more precise mathematical foundations and obvious physical explanation. In this study, the Q criterion is applied to investigate vortex shedding around the pile in addition to vortices results. The Q criterion is estimated as follows:

$$Q = \frac{1}{2}\left(\|\Omega\|^2 - \|S\|^2\right) \tag{10}$$

where Ω is the rate-of-rotation tensor corresponding to the pure rotational motion and equals to

$$\Omega = \frac{1}{2}\left[\nabla U - (\nabla U)^T\right] \tag{11}$$

and S is the rate-of-strain tensor corresponding to the pure irrotational motion and equals to

$$S = \frac{1}{2}\left[\nabla U + (\nabla U)^T\right] \tag{12}$$

where U is the velocity vectors in three-dimensional Cartesian coordinate and, ∇U is the full local velocity gradient tensor.

In Figure 10, Q criterion variations around the pile at a specific instant time for all cases are depicted. In this figure, $\omega t = 90^\circ$ (left-hand side panel) and $\omega t = 270^\circ$ (right-hand side panel) mean pile is located in the crest and trough half-period, respectively. Therefore, for the former one, horseshoe vortices is formed in the left-hand side of the pile and lee-wake vortices is formed in the right-hand side of the pile. For the latter one, horseshoe vortices is formed in the right-hand side of the pile and lee-wake vortices is formed in the left-hand side of the pile. Regarding to Figure 10, there is no lee-wake vortices when KC= 2.8. By increasing KC to more than 6.0, horseshoe vortices are formed in front of the pile and symmetric lee-wake vortices behind the pile. In addition to horseshoe vortices in front of the pile, at KC= 10.3 and KC= 20.1, the vortex shedding are occurred behind the pile. It can be seen that when KC is very small, the horseshoe vortex may not even be formed. Instead, for the large KC the flow in each half-period is similar to when steady current, which are in line with Sumer et al. results [1]. In addition to Q criterion, the vorticity field is investigated for all cases. Here, vorticity in different stage during one wave period for case 4 (KC= 20.1) is depicted to show the generation and suppression of vortex shedding as well as its impact on the wave force due to increasing disturbance. Figure 11 shows the vorticity in every T/22 time step (= 0.2 sec) during one wave period for case 4 (KC= 20.1).

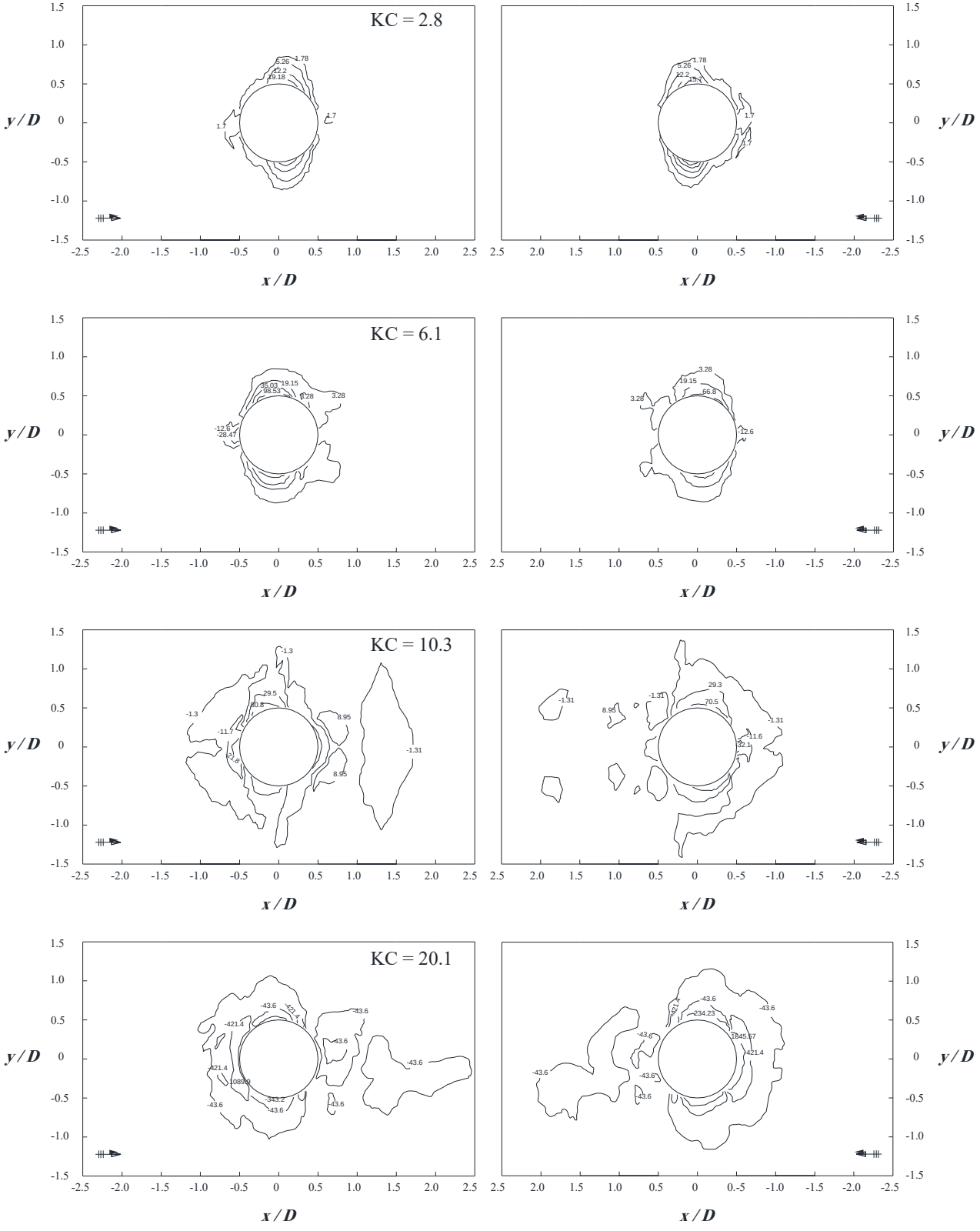

Figure 10. *Q* Criterion around the pile at the bottom of the wave tank at a selected instant of time ($\omega t = 90^{\circ}$ for the left-hand side pictures and $\omega t = 270^{\circ}$ for the right-hand side pictures)

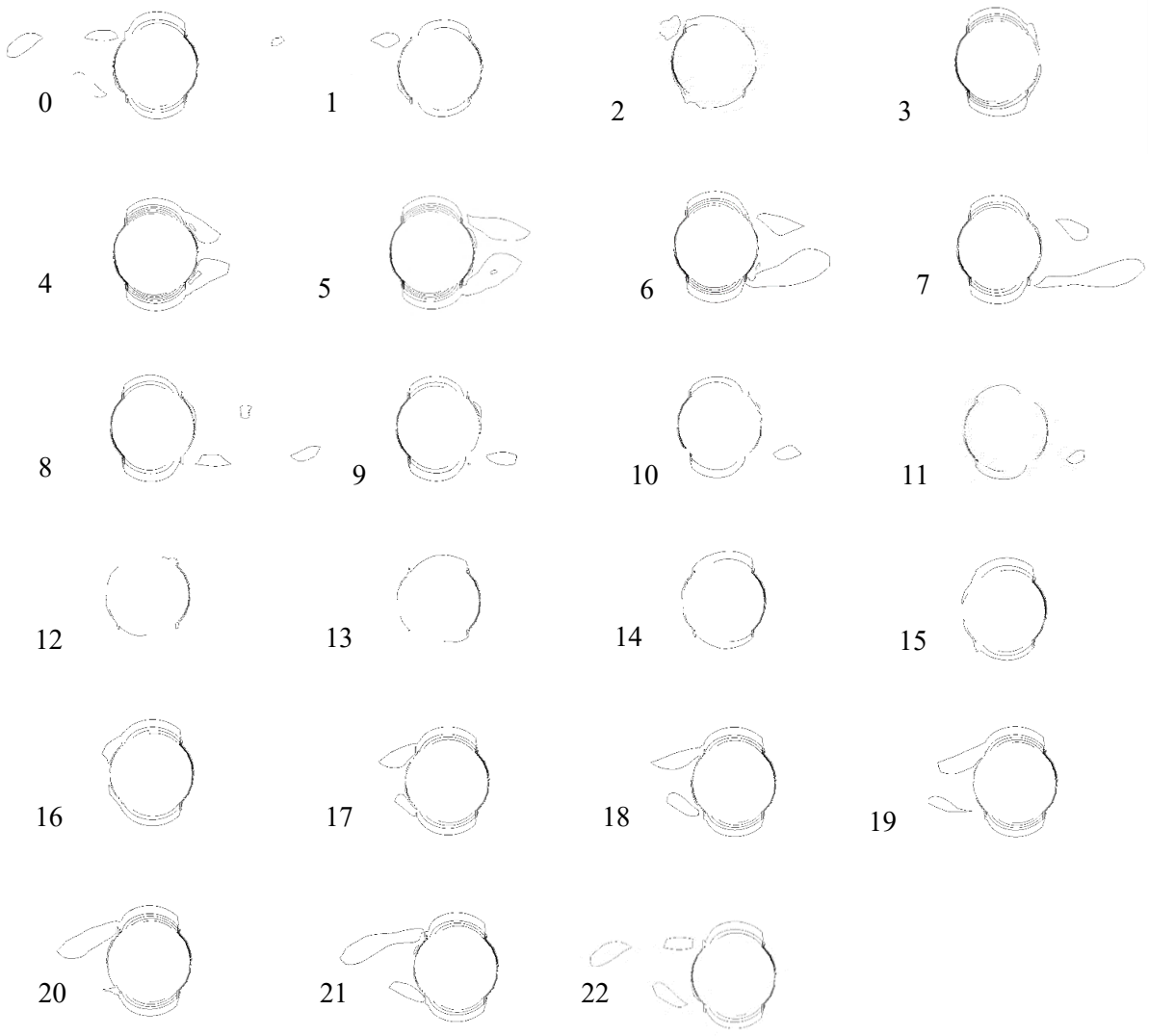

Figure 11. Vorticity snap shot during one wave period for case 4 (KC= 20.1)

In the figure, the pile is in the crest half-period at stage 0, and remaining vortices from previous stage in up-stream side are damped suddenly due to Cnoidal wave shape in crest half period. After a short while lee-wake vortices are generated and vortex shedding happened, from time stage 4. This is continuing to the flow direction changed and pile would be in trough half-period at stage 7. But, vortex shedding is still happening and vortices are being separated from the flow. Following the flow reversal, downstream vortices pushed back and hit on the pile, which is the main reason for existence of some disturbance in the total in-line force acting on pile in trough half-period. To comprehend more, variation of the total in-line force acting on pile for case 4 (KC= 20.1) corresponding to time stages of Figure 11 is depicted in Figure 12. Considering simultaneously both figures, the existence of small pick point in the trough half-period through time stage 7 to 11 is approved. This is happening up to time stage 12, when the vortex shedding is damped and the flow direction totally is changed. As seen from Figure 11, after that time the vortex shedding is reversal to the pile and the trend continues.

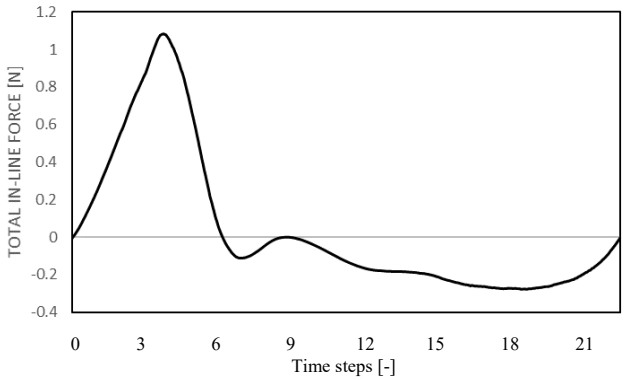

Figure 12. Total in-line force acting upon pile variation in one wave period for case 4 (KC=20.1)

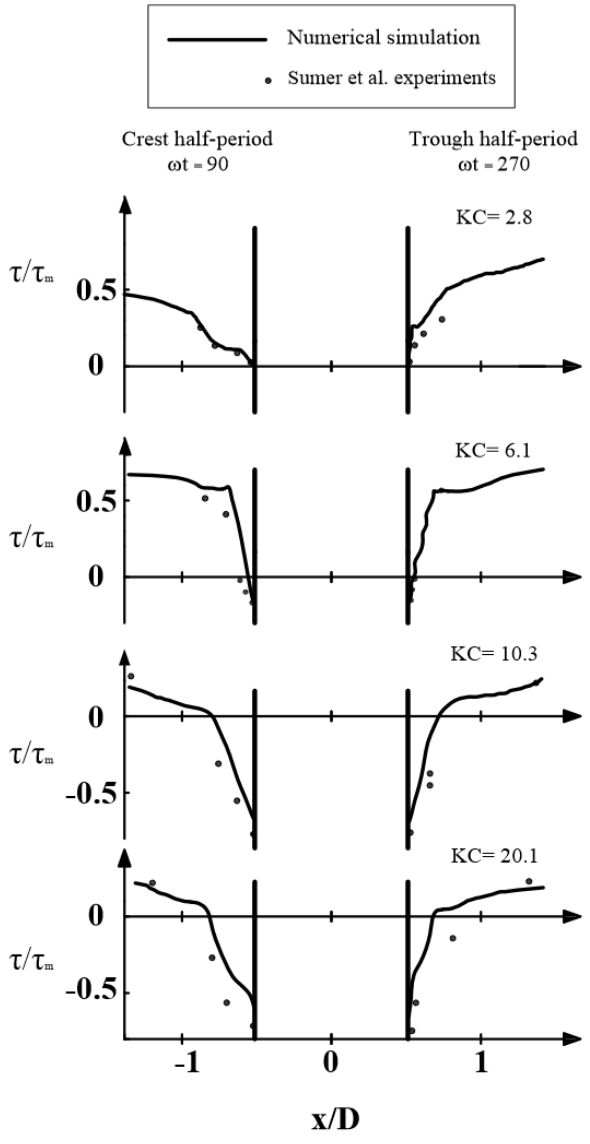

Figure 13. Variation of bed shear stress along x axes near the pile at crest half-period ($\omega t = 90^{\circ}$) and trough half-period ($\omega t = 270^{\circ}$) for all cases

Generation of horseshoe vortex around the pile affect the bed shear stress and consequently the sediment transport potential and scour around the pile. The numerical results showed that the bed shear stress increases with increasing KC, which can be consequence of the increased presence of the horseshoe vortices. The bed shear stress is expressed by means of amplification factor

$$\alpha = \frac{\tau}{\tau_{\infty}} \tag{13}$$

where τ refers to the bed shear stress and τ_{∞} is the bed shear stress for the undisturbed flow. Bed shear stress beneath the horseshoe vortex was investigated and it is concluded that when no negative bed shear stress near the pile exist, no horseshoe vortex exists either. The numerical model results are in line with Sumer et al. statement [1]. Figure 13 illustrates variation of bed shear stress along x axis near the pile at the crest half-period ($\omega t = 90^{\circ}$) and the trough half-period ($\omega t = 270^{\circ}$) for all cases. As seen, for Case 1 (KC=2.8) no horseshoe vortex formed as no negative bed shear stress existed for both wave phase, which is along with obtained results by investigating the vorticity and *Q* criterion. In Case 2 (KC= 6.1) the bed shear stress near the pile have some negative values, which is result of generating horseshoe vortices there. By increasing KC for Case 3 and 4 the magnitude of negative values of bed shear stress in vicinity of the pile increased, which implies the horseshoe vortices are completely formed.

5. Conclusions

Three-dimensional numerical simulation of regular waves passing over a cylindrical pile was carried out to investigate the hydrodynamic force acting on pile as well as vortex dynamics around that. The open-source CFD toolkit OpenFOAM, which combines the Eulerian multi-fluid approach, was applied to model the rectangular wave flume and monopile.

Some numerical results were compared to the experimental ones to validate the model e.g. water particle velocity at a wave gauge, the surface elevation at four wave gauges, the total in-line force acting on the pile and the time histories of dynamic pressure along the perimeter of the pile in six angular points.

Four cases with different KC number were modeled to investigate on hydrodynamic in-line force acting on pile and the vortex dynamics around the pile. The vorticity field around the pile was investigated as well as vortices by means of *Q* criterion. From the numerical investigation, the following conclusions are drawn:

- Variation of KC number has different impacts on the hydrodynamic in-line force acting on pile. That is, change in KC due to change in *T* did not significantly influence on the hydrodynamic in-line force acting on pile. While, it remarkably increased for increasing KC due to change in *H*.
- In vortex shedding regime, drag force component increased and inertia force component decreased.

- Some pick points in negative values of the total in-line force acting on the pile were seen, which can be due to vortex shedding behind the pile and consequently increasing of disturbance around that.
- The bed shear stress near the pile when KC >6 is negative which is the result of existence of horseshoe vortices. By increasing KC up to 20, the magnitude of negative values of bed shear stress near the pile increased which implies horse shoe vortices were completely formed.

6. References

1- Sumer, B. M., Christiansen, N., & Fredsøe, J. (1997). The horseshoe vortex and vortex shedding around a vertical wall-mounted cylinder exposed to waves. *Journal of Fluid Mechanics*, *332*, 41-70.

2- Iwagaki, Y., & Ishida, H. (1976). Flow separation, wake vortices and pressure distribution around a circular cylinder under oscillatory waves. *Coastal Engineering Proceedings*, *1*(15).

3- Morgan, G. C. J., Zang, J., Greaves, D., Heath, A., Whitlow, C., & Young, J. (2011). Using the rasInterFoam CFD model for wave transformation and coastal modelling. *Coastal Engineering Proceedings*, *1*(32), 23.

4- Amini Afshar, M. (2010). Numerical wave generation in Open FOAM®.

5- Baykal, C., Sumer, B. M., Fuhrman, D. R., Jacobsen, N. G., & Fredsøe, J. (2015). Numerical investigation of flow and scour around a vertical circular cylinder. *Philosophical Transactions of the Royal Society of London A: Mathematical, Physical and Engineering Sciences*, *373*(2033), 20140104.

6- oM, W., Irschik, K., Oumeraci, H., & Liu, P. L. F. (2007). A 3D numerical model for computing non-breaking wave forces on slender piles. *Journal of Engineering Mathematics*, *58*(1), 19-30.

7- Jacobsen, N. G., Fuhrman, D. R., & Fredsøe, J. (2012). A wave generation toolbox for the open-source CFD library: OpenFoam®. *International Journal for Numerical Methods in Fluids*, *70*(9), 1073-1088.

8- Benitz, M. A., Schmidt, D. P., Lackner, M. A., Stewart, G. M., Jonkman, J., & Robertson, A. (2014, June). Comparison of hydrodynamic load predictions between reduced order engineering models and computational fluid dynamics for the oc4-deepcwind semi-submersible. In *ASME 2014 33rd International Conference on Ocean, Offshore and Arctic Engineering* (pp. V09BT09A006-V09BT09A006). American Society of Mechanical Engineers.

9- Higuera, P., Lara, J. L., & Losada, I. J. (2013). Simulating coastal engineering processes with OpenFOAM®. *Coastal Engineering*, *71*, 119-134.

10- Paulsen, B. T., Bredmose, H., & Bingham, H. B. (2014). An efficient domain decomposition strategy for wave loads on surface piercing circular cylinders. *Coastal Engineering*, *86*, 57-76.

11- Stahlmann, A. (2013, June). Numerical and experimental modeling of scour at foundation structures for offshore wind turbines. In *The Twenty-third International Offshore and Polar Engineering Conference*. International Society of Offshore and Polar Engineers.

12- Paulsen, B. T., Bredmose, H., Bingham, H. B., & Jacobsen, N. G. (2014). Forcing of a bottom-mounted circular cylinder by steep regular water waves at finite depth. *Journal of fluid mechanics*, *755*, 1-34.

13- Jiang, C., Yao, Y., Deng, Y., & Deng, B. (2015). Numerical Investigation of Solitary Wave Interaction with a Row of Vertical Slotted Piles. *Journal of Coastal Research*, *31*(6), 1502-1511.

14- Haddorp, R. (2005). Predictability of Scour at Large Piles due to Waves and Currents.

15- Sumer, B. M. (2002). *The mechanics of scour in the marine environment* (Vol. 17). World Scientific Publishing Company.

16- Hoffmans, G.J.C.M., Verheij, H.J. (1997): "Scour Manual", Rotterdam.

17- Coastal Engineering Manual (2003): "EM 1110-2-1100 (Part VI) ", Chapter 5, p.242-245, Washington.

18- Isaacson, M. (1979). Wave-induced forces in the diffraction regime. *Mechanics of wave-induced forces on cylinders*.

19- Menter, F. R. (1994). Two-equation eddy-viscosity turbulence models for engineering applications. *AIAA journal*, *32*(8), 1598-1605.

20- WILCOX, D. (1988). Reassessment of the scale-determining equation for advanced turbulence models. *AIAA journal*, *26*(11), 1299-1310.

21- Hirt, C. W., & Nichols, B. D. (1981). Volume of fluid (VOF) method for the dynamics of free boundaries. *Journal of computational physics*, *39*(1), 201-225.

22- Jacobsen, N. G. (2017). waves2Foam Manual.

23- OS, D. (2011). J101, Design of Offshore Wind Turbine Structures. *DET NORSKE VERITAS AS, Ausgabe*, *9*.

24- Chen, Q., Zhong, Q., Qi, M., & Wang, X. (2015). Comparison of vortex identification criteria for planar velocity fields in wall turbulence. *Physics of Fluids*, *27*(8), 085101.

25- Sumer, B. M. (2006). *Hydrodynamics around cylindrical structures* (Vol. 26). World scientific.